Effect of magnetic coupling on the magnetization reversal in arrays of magnetic nanocaps

T. C. Ulbrich,[1] C. Bran,[2] D. Makarov,[3,*] O. Hellwig,[4] J. D. Risner-Jamtgaard,[4] D. Yaney,[4] H. Rohrmann,[5] V. Neu,[2] and M. Albrecht[3]

[1]*Department of Physics, University of Konstanz, D-78457 Konstanz, Germany*

[2]*Institute for Metallic Materials, IFW Dresden, D-01069 Dresden, Germany*

[3]*Institute of Physics, Chemnitz University of Technology, D-09107 Chemnitz, Germany*

[4]*Hitachi Global Storage Technologies, San Jose Research Center, 3403 Yerba Buena Road, San Jose, California 95135, USA*

[5]*OC Oerlikon Balzers AG, FL-9496 Balzers, Liechtenstein*

(Received 5 November 2009; published 17 February 2010)

Magnetic $[Co/Pd]_N$ multilayers grown on assemblies of spherical polystyrene particles were used as a model system for studying the influence of magnetic coupling on the magnetization reversal by changing the size of the nanoparticles as well as the total thickness of the deposited magnetic film. The coercive field and the switching field distribution are found to be strongly dependent on the size of the nanocaps and on the total thickness of the magnetic layer, indicating a strong influence of the magnetic dipole-dipole interaction on the magnetization reversal of the entire array of nanocaps. Moreover, magnetic viscosity measurements allowed the estimation of the magnetic activation volume representing the effect of thermal activation on the switching process. It was found that the magnetic activation volume is substantially smaller compared to the volume of the nanocap and almost independent of the number of bilayers, and thus the total thickness of the nanocap, supporting an inhomogeneous magnetization reversal process.

DOI: 10.1103/PhysRevB.81.054421 PACS number(s): 75.70.Cn, 75.60.Jk, 75.70.Kw

I. INTRODUCTION

The tremendous development in mass fabrication of nanoparticles enabled their utilization for various applications. Prominent examples are the creation of high-efficiency hybrid solar cells[1,2] and sensoric applications for pathogen detection.[3,4] Another important field is the potential of magnetic nanostructures as future magnetic recording media.[5–10] Current conventional granular storage media are facing the superparamagnetic limit[7,9] and in order to keep future growth in areal density, new recording concepts are required. In this respect, the most promising candidate is the bit-patterned media (BPM) scheme where an individual bit will be stored in a single magnetic volume. Suitable materials for BPM are films with strong out-of-plane magnetic anisotropy, i.e., Co/Pt and Co/Pd multilayers[10] as well as hard magnetic FePt and CoPt alloys.[8,9] In order to provide an areal density of 1 Tbit/in.^{2} utilizing the BPM concept, an assembly of 10 nm bits in a regular lattice with a period of 25 nm has to be achieved.[8] However, at such small distances the magnetostatic interactions between the neighboring nanostructures increase drastically thus influencing substantially the magnetization reversal process.[11]

To explore the effect of magnetic coupling on the reversal behavior in an array of nanostructures, we have considered a bottom-up process to obtain a nanosized system by deposition of magnetic films onto assemblies of spherical nanoparticles.[12–15] In these magnetic cap arrays, the magnetic exchange and magnetostatic interaction can be easily tuned by varying the particle diameter as well as the thickness of the deposited magnetic film.[16] For instance, changing the size of the particles allows studying the scaling dependence of the coercive field and switching field distribution (SFD). In this respect, the main contribution to the SFD is given by the particle size distribution. However, at small separation distances between nanostructures, the dipole-dipole interaction becomes rather important and will strongly influence the magnetization reversal in the array.[11] Likewise, large film thicknesses in the range of the particle diameter may also result in direct exchange coupling of neighboring nanostructures. Therefore, a detailed study of the magnetization reversal behavior of different particle arrays covered by $[Co/Pd]_N$ multilayer stacks with varying bilayer number N exhibiting an out-of-plane easy axis of magnetization will be presented.

II. EXPERIMENTAL DETAILS

Monolayers of hexagonal closed-packed polystyrene particle assemblies with particle diameters of 58 and 110 nm were prepared following a conventional routine proposed by Micheletto *et al.*[17] The particle arrays were covered with $[Co(0.27\ nm)/Pd(0.8\ nm)]_N$ multilayers consisting of different numbers of bilayers, N, ranging between 8 and 80. The deposition of Co/Pd multilayer stacks was performed by magnetron sputtering using Kr as a sputter gas at a pressure of 3.9×10^{-2} mbar. In order to improve the growth condition of the multilayers, a 5-nm-thick Pd buffer layer was sputtered (3.9×10^{-2} mbar of Kr pressure) onto a 1-nm-thick Cr seed layer (3.5×10^{-3} mbar of Ar pressure) grown directly on the particles. A 1-nm-thick Pd capping layer was deposited to protect the multilayer stacks from oxidation. In addition, a series of reference samples was prepared on planar glass substrates for comparison.

The magnetic properties of the samples were investigated using polar magneto-optical Kerr effect magnetometry (P-MOKE), vibrating sample magnetometry (VSM), and magnetic force microscopy (MFM). The structural properties were analyzed by transmission electron microscopy (TEM, JEOL 2010F, 197 keV) in cross-section mode on lamellas

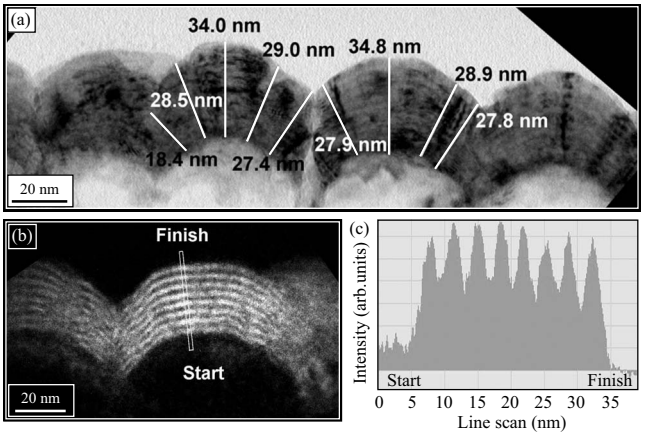

FIG. 1. TEM images of an assembly of SiO_2 particles with a size of nominally 50 nm covered with a [Co (1.8 nm)/Pd(1.8 nm)]$_8$ multilayer stack: (a) bright-field cross-sectional image. The thickness variation in the film with varying angle is indicated. (b) Energy filtered image (only Co layers are visible as the bright layers). (c) Intensity profile taken along the line marked in (b).

prepared by focused ion beam (FIB). In order to protect the area of interest during FIB preparation, the site was coated with SiO_x and tungsten. However, imaging of Co/Pd multilayer stacks with rather thin individual layers is a challenging task. Therefore, an additional sample, [Co(1.8 nm)/Pd(1.8 nm)]$_8$, with thicker individual Co and Pd layers was prepared on nominally 50 nm SiO_2 particles. However, a comparison of the Co/Pd microstructure when grown on polystyrene particles has to be taken with care.

A cross-section bright-field TEM image taken on this sample is shown in Fig. 1(a) revealing the film morphology on top of the 50 nm particle assembly. Since the particles were sliced approximately at the center, the film thickness at the top of the cap is approximately at the multilayer nominal film thickness, which is about 34 nm, but it continuously varies along the surface due to the spherical topography, being thicker at the top and thinner close to the particle equator. For these particles, the film thickness is almost comparable to the particle radius. High-resolution TEM imaging exhibits a polycrystalline fcc structure with a weak texture. The grains forming the cap have a mean lateral size of approximately 15 nm. Notice that although the particles act as a curved substrate, the film remains rather continuous at least for this film thickness.

In order to get a better insight in the stacking of the multilayer, layer-resolved electron-energy-loss spectroscopy measurements were performed. The analysis of the energy-filtered TEM image reveals a clear multilayer contrast at the central part of the nanocaps [Figs. 1(b) and 1(c)]. However due to the curved topography, where the film deposition is almost grazing to the particle surface, the film close to the particle equator becomes inhomogeneous concerning the multilayer structure and interface definition. In particular at the intersections some granular structure arises and the Co/Pd interfaces are no longer visible, thus forming a Co-Pd mixture [Fig. 1(b)]. Dependent on the composition, the magnetic properties of the Co-Pd alloy differ substantially from the properties of Co/Pd multilayers. Note that for the case of [Co(0.27 nm)/Pd(0.8 nm)] multilayers with a rather thin Co layer the formation of a Pd-rich Co-Pd alloy with a Curie temperature below 300 K is expected.[18,19] In this case, although the neighboring nanocaps are interconnected, the interface region possesses paramagnetic properties leading to strong exchange isolation of the neighboring nanocaps in the array.[12,13,16] However, this decoupling mechanism will weaken with increasing number of bilayers, in particular, when the total film thickness is in the range of half the particle diameter.

A further important aspect is the fact that the Co/Pd interfaces are following the curvature of the particle top surface resulting in radially oriented grains [lines in Fig. 1(a)] as also reported by Soares *et al.*[14] This behavior has an important consequence on the magnetic properties of the nanocap structure: As the out-of-plane easy axis of magnetization in Co/Pd multilayer films is driven by the interface anisotropy,[20,21] a tilt in the growth direction of the stack will result in a deviation of the easy-axis orientation following the curvature of the particle's surface as well. This idea of a spread of the anisotropy axis across the surface with the average anisotropy axis pointing along the deposition direction was already utilized to explain the modification in magnetization reversal behavior of Co/Pt(Pd) multilayers grown on particle assemblies.[12,13]

From the TEM analysis, it becomes clear, that the use of nanocap arrays provides an interesting route to alter the inner structure by simply changing the relative dimensions between the film thickness and the particle size thus allowing to studying systematically magnetic coupling phenomena in nanosized systems.

III. RESULTS AND DISCUSSION

P-MOKE hysteresis loops of the reference samples are summarized in Fig. 2(a). The shape of the loops with its sudden strong decrease in magnetization above a certain reverse field indicates that the magnetization reversal process is governed by nucleation followed by domain-wall propagation. An initial increase in the coercive field was observed when the number of bilayers N of the Co/Pd multilayer increased from 8 to 16 but then levels off for larger bilayer numbers. This behavior can be explained with an enhancement of the magnetic anisotropy which scales with the number of Co/Pd interfaces.[22,23] However, with an increase in the bilayer number the amount of structural defects affecting the interface quality also increases, resulting in an overall reduction in the magnetic anisotropy. Please note that increase in the number of bilayers affects not only the magnetic anisotropy value but also influences the propagation of magnetic domain walls in the film and thus the coercivity. In addition, it is important to mention that with increasing bilayer number the stray fields become larger which leads to the stabilization of specific domain configurations, such as bubble domains exhibiting a higher saturation field as indicated by the occurrence of an additional high-field tail in the hysteresis loops. This feature is in agreement with observations reported earlier on Co/Pt(Pd) multilayers.[24,25]

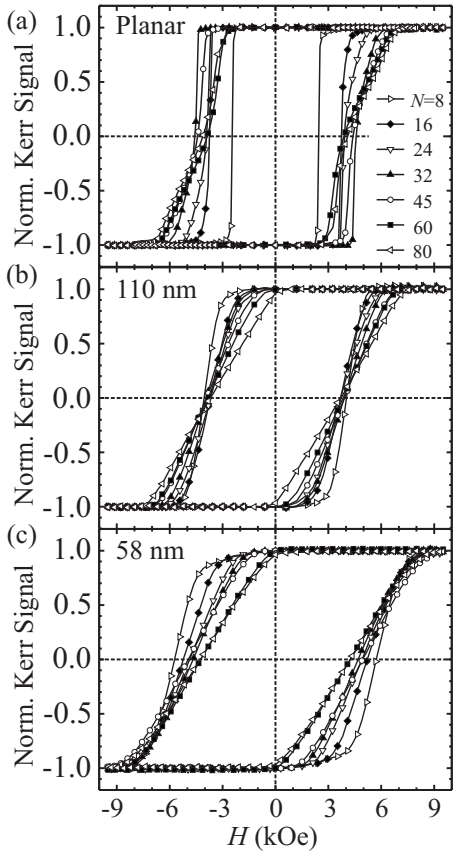

FIG. 2. Series of P-MOKE hysteresis loops of $[Co/Pd]_N$ multilayer stacks with different bilayer number N grown on (a) a planar substrate, (b) an assembly of 110 nm particles, and (c) an assembly of 58 nm particles.

Hysteresis loops measured on Co/Pd multilayers grown on assemblies of particles are presented in Figs. 2(b) and 2(c). A systematic shearing of the hysteresis loops with increasing number of bilayers is observed indicating the influence of the dipolar fields originating from neighboring magnetic caps. Furthermore, the variation in H_C in the films grown on the particle assemblies with the number of bilayers is different compared to the observation on the planar substrates. Thus, Co/Pd multilayers on assemblies of particles with a diameter of 110 nm possess a rather constant coercivity independent of the number of bilayer N [Fig. 2(b)]. This might be related to the different microstructure of a multilayer stack grown on particles compared to planar substrates. The absolute value of coercive field is however close to the one observed on the planar substrates. In the case of the films grown on 58 nm particles [Fig. 2(c)] a remarkable increase in the out-of-plane coercivity compared to the deposits on 110 nm particles [Fig. 2(b)] as well as on the planar substrates is observed for the smallest bilayer number. However, with the increase in the bilayer number, the coercivity gradually decreases to a value of 4.5 kOe which might be related to the degradation of the interface quality for the thicker films as mentioned earlier. Following this assumption, a variation in the magnetic anisotropy constant with the film thickness might be expected resulting in a reduction in the coercive field as revealed by micromagnetic simulations.

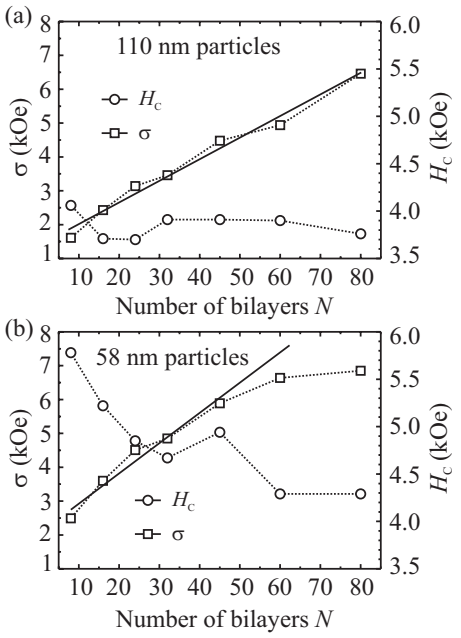

FIG. 3. The evolution of switching field distribution, σ, and out-of-plane coercivity, H_C, with bilayer number for $[Co/Pd]_N$ samples grown on assemblies of (a) 110 nm and (b) 58 nm particles. Dotted lines are guides to the eye. Linear fits to the SFD data are also shown with solid lines.

In addition, magnetostatic interaction between the neighboring caps will also cause a reduction in coercive field.[11]

The evolution of the coercive field H_C and the width σ of the SFD with the number of Co/Pd bilayers in the multilayers grown on particle assemblies is summarized in Fig. 3. The values of H_C and σ are close to the ones reported by Thomson *et al.*[26] for lithographically patterned Co/Pt multilayer films. The SFD is given as the full width at half maximum of the first derivative of the hysteresis loop fitted with a Gaussian distribution function. In addition to the intrinsic SFD arising from the inner defect structure of the Co/Pd multilayers, the broadening of the SFD is given by the particle size distribution as well as by the influence of the dipolar fields coming from the neighboring caps.[26,27] In our case, the distribution of the particle sizes in the array plays initially the major role, however with increasing number of bilayers, the width σ of the SFD increases linearly which is attributed to the effect of dipolar fields, which increases proportionally with the growing total magnetic moment of each nanocap. By comparing the evolution of the SFD with increasing bilayer number for the particle arrays it becomes apparent that the SFD increases for the 58 nm array with a steeper slope (88 Oe per bilayer) than for the 110 nm array (64 Oe per bilayer), which is expected due to larger dipolar fields for smaller interparticle distances. Extrapolating the linear fit to the intersection with y axis, we extracted the intrinsic SFD, σ_0, without magnetostatic contribution. As expected, owing to the larger particle size distribution, the value for σ_0 for the deposits on 58 nm particle arrays was found larger (2.1 kOe) compared to the films grown on assemblies of 110 nm particles (1.4 kOe). Interestingly the linear increase in the SFD starts to level off when the total film

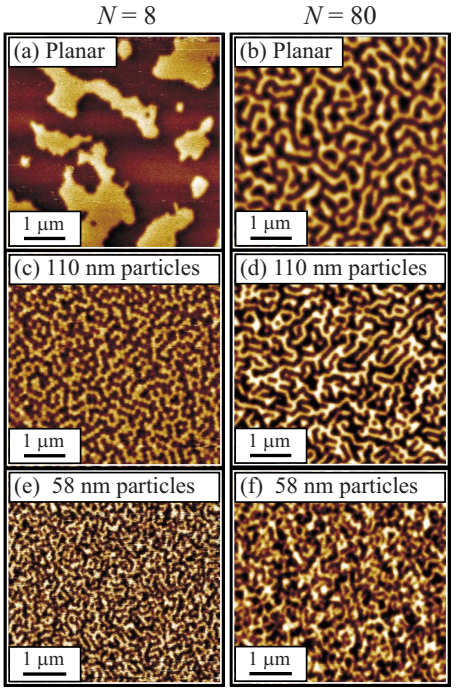

FIG. 4. (Color online) MFM images taken in the demagnetized state for $[Co/Pd]_N$ samples with $N=8$ and 80 grown on [(a) and (b)] a planar substrate, [(c) and (d)] assemblies of 110 nm particles, and [(e) and (f)] assemblies of 58 nm particles.

thickness is in the range of the particle diameter ($N>50$), thus probably indicating the onset of enhanced exchange coupling in the array.

For investigating the magnetic properties of the samples on the local scale, magnetic force microscope imaging was performed. In addition to measurements at remanence after applying different field treatments to the samples, an in-field study was carried out using a home-built magnetic stage.[28] The MFM images on the reference samples measured in the ac-demagnetized state are presented in Figs. 4(a) and 4(b). While the film sample with $N=8$ bilayers reveals large domains on the order of several micrometers [Fig. 4(a)], a labyrinthlike domain pattern appears for film samples with larger bilayer number, accompanied with a substantial reduction in the domain size down to about 200 nm [Fig. 4(b)]. The domain size observed for the two different film thicknesses is in agreement with the magnetic domain theory of Málek *et al.*[29] and has been experimentally observed in comparable multilayer films.[30]

In contrast, the MFM images taken on the samples grown on particle assemblies show a well-defined black and white contrast on individual caps confirming that the caps are in a single domain state. Note that as the demagnetized state of the sample is driven by magnetostatic interactions, a labyrinthlike overall domain pattern is observed [Figs. 4(c)–4(f)]. Interestingly, the domain size is independent of the number of bilayers in a stack, as the magnetic domains are localized at the cap structures even for $N=80$. This observation is quite surprising considering the total film thickness compared to the particle diameter, where the issue of exchange coupling between caps may become especially important.

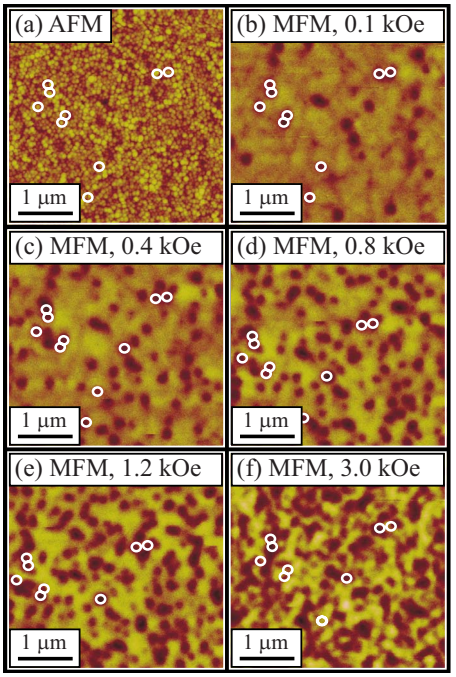

FIG. 5. (Color online) (a) AFM image taken for the $[Co/Pd]_N$ sample with $N=80$ grown on 58 nm particles. [(b)–(f)] Series of MFM images taken after exposure of the initially saturated sample to an increasing reverse magnetic field.

To get a better understanding on the magnetization reversal process of the 58 nm particle sample with $N=80$, an in-field MFM study was carried out (Fig. 5). Therefore, the initially saturated sample was imaged in a reverse perpendicular magnetic field. The MFM image taken at a reverse field of 0.1 kOe [Fig. 5(b)] shows a few isolated areas (dark contrast, some marked with a white circle), corresponding to nanocaps in a magnetic single domain state with magnetization direction opposite to the surrounding area. Increasing the applied reverse field results in a successive switching of individual magnetic nanocaps [Figs. 5(c)–5(f)]. In addition to single switching events, the reversal of entire regions consisting of several nanocaps is observed. It is suggested that preferential nucleation will take place at defect sites revealing low anisotropy as present at the intersections of the particle caps. In this respect, atomic force microscopy (AFM) imaging still reveals well-separated cap structures even for $N=80$ on assemblies of particles with a size of 58 nm [compare Figs. 6(a) and 6(b)]. However, with increasing number of bilayers larger grains are formed on individual particles [Fig. 6(b)], which might result in an enhanced number of effective nucleation/pinning sites for domain walls.[31] Therefore, despite the presence of exchange coupling throughout the array, individual switching events located at cap positions can still occur followed by depinning of domain walls or further nucleation depending on the intrinsic magnetic properties and the specific local magnetic environment. Similar results were reported for CoPt alloys deposited onto particle arrays.[32]

IV. RELAXATION/VISCOSITY MEASUREMENTS

An additional insight into the magnetization reversal can be gained from integral magnetization measurement by esti-

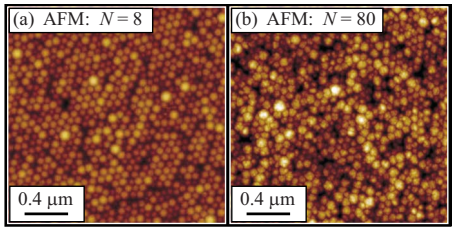

FIG. 6. (Color online) AFM images taken for $[Co/Pd]_N$ samples with (a) $N=8$ and (b) $N=80$ grown on assemblies of 58 nm particles.

mating the volume involved in the switching process (the so-called activation volume) via measurements of the fluctuation field, H_F, using VSM. The latter expresses the effect of thermal activation on the switching process in terms of an equivalent field,[33] thus allowing to calculate not only the activation volume but also the thermal stability factor $\beta = \Delta E/k_B T$. This quantity compares the energy barrier against magnetization reversal, ΔE, with the thermal energy, $k_B T$, at a given temperature T and is therefore important to test the applicability of the Co/Pd multilayers grown on particle assemblies as a potential magnetic storage media.

Following the theory by Wohlfarth *et al.*,[34] the fluctuation field, H_F, in systems with large energy barrier distribution can be expressed as,

$$H_F(H) = S(H)/\chi_{irr}(H) \tag{1}$$

with $S(H)$ and $\chi_{irr}(H)$ being the magnetic viscosity and the irreversible susceptibility, respectively. $S(H)$ is determined

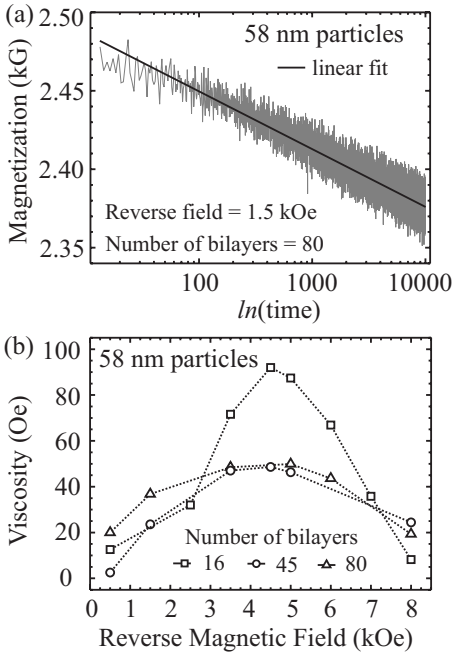

FIG. 7. $[Co/Pd]_N$ samples grown on 58 nm particles. (a) Magnetization relaxation data taken in the reverse field of 1.5 kOe for the sample with $N=80$. (b) Magnetic viscosity as a function of the reverse magnetic field, H, for $[Co/Pd]_N$ samples with $N=16$, 45, and 80. The samples were initially magnetized at 30 kOe. Dotted lines are guides to the eye.

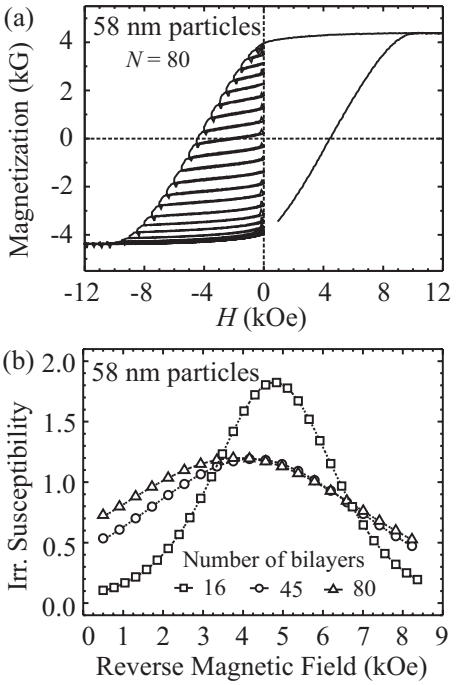

FIG. 8. $[Co/Pd]_N$ samples grown on 58 nm particles. (a) Series of recoil loops measured on the sample with $N=80$. (b) Irreversible susceptibility as a function of the reverse magnetic field, H, for $[Co/Pd]_N$ samples with $N=16$, 45, and 80. The samples were initially magnetized at 30 kOe. Dotted lines are guides to the eye.

from magnetization relaxation measurements, where the time-dependent magnetization $M(t;H)$ is measured in a constant reverse field H applied to the initially saturated sample. The large energy barrier distribution guarantees a linear dependence of $M(t;H)$ on the logarithm of time over a large time interval,[35]

$$M(t;H) = \text{const} - S(H)\ln t. \tag{2}$$

For time-dependent measurements the particle samples with $N=16$, 45, and 80, were first saturated at 30 kOe before applying a reverse magnetic field. At each applied reverse field, H, the magnetic moment was measured for 9999 s. The magnetization relaxation follows a logarithmic time dependence over the entire range investigated [Fig. 7(a)], as expected for samples with a broad SFD (Fig. 3).[35] The magnetic field dependence of the viscosity, $S(H)$, was determined by fitting the measured $M(t;H)$ curves according to Eq. (2) [Fig. 7(b)]. The viscosity curves show a broad field dependence with a maximum close to the coercive field, where the energy barrier for magnetization reversal is near zero. With the decrease in the bilayer number to $N=16$, the maximum of the magnetic viscosity drastically increases.

The irreversible susceptibility, $\chi_{irr}(H)$, is derived from recoil loops [Fig. 8(a)] by measuring the remanent magnetization in the demagnetizing branch, $M_r^d(H)$, as a function of the former reverse field H applied to the saturated sample. The irreversible susceptibility, $\chi_{irr}(H)$, for the same set of samples is shown in Fig. 8(b). The data reveals similar field dependence compared to the viscosity measurements with a pronounced peak around the coercive field. Furthermore, the

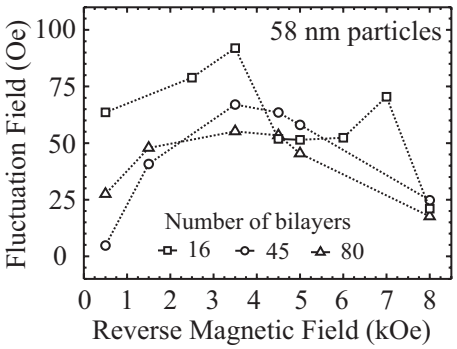

FIG. 9. Fluctuation field as a function of the negative applied field for $[Co/Pd]_N$ samples with $N=16$, 45, and 80. Dotted lines are guides to the eye.

maximum on the $\chi_{irr}(H)$ dependence scales in a similar way with the number of bilayers, N, as found for the viscosity.

Combining the magnetic viscosity and irreversible susceptibility measurements [Eq. (1)], we deduce the magnetic field dependence of the fluctuation field, $H_F(H)$. Although both, viscosity and irreversible susceptibility data reveal a strong magnetic field dependence, the fluctuation field is found to be almost independent of H as well as on the number of bilayers around the coercivity but tail off at lower and higher fields (Fig. 9, Table I). The derived values $H_F(H_C;N)$ were used to extract the activation volume governing the reversal process,[34]

$$V_{act} = k_B T/(M_S H_F). \tag{3}$$

Despite the large change in the number of bilayers, N, the activation volume is rather constant and does not scale with the total film thickness (Table I). It furthermore adopts a value of about 2000 nm^3, which is substantially smaller than the physical volume of an individual nanocap (Table I). The latter is in agreement with the observed individual reversal of magnetic nanocaps (Figs. 5 and 6) indicating the exchange decoupling between the neighboring nanocaps in the array. Moreover, the finding $V_{act} \ll V_{cap}$ further suggests an inhomogeneous magnetization reversal process rather than a coherent switching within the individual nanocaps for which $V_{act} \approx V_{cap}$ is expected. This finding is in agreement with results obtained by micromagnetic simulations.[13]

In order to relate the estimated value of the activation volume to the physical volume relevant for the system under consideration, we have to account for the angular modification of magnetic parameters. According to the discussion above, the thickness of individual layers changes with angle resulting in a gradual transformation of the Co/Pd multilayer stack to a Co-Pd alloy influencing the magnetic anisotropy constant (K_U^0), saturation magnetization (M_S^0), as well as exchange parameter (A^0). The further estimations will be performed assuming the following angular dependence of the relevant magnetic parameters,[13]

$$K_U(\theta) = K_U^0 \times f(\theta), \quad M_S(\theta) = M_S^0 \times f(\theta),$$

$$A(\theta) = A^0 \times f(\theta)^2 \tag{4}$$

with $f(\theta)=\exp[-(\theta-\theta_0)^2/\Delta^2]$ for $\theta > \theta_0$. Here Δ is the half width of the distribution and the angle, $\theta_0 \approx 50°$, is related to the reduction in the thickness of an individual Co layer below a certain critical thickness where the degradation of magnetic properties of magnetic multilayers occurs. In this case, the width of a Bloch domain wall can be expressed as $d_{BW}(\theta)=d_0 \times f(\theta)$, where $d_0=18$ nm is the typical domain-wall width in Co/Pd multilayer films ($M_S^0=6.3$ kG, $K_U^0=3 \times 10^5$ erg/cm^3, and $A^0=10^{-6}$ erg/cm). Assuming an isotropic nucleation process, the activation volume can be expressed as

$$V_{act} \approx d_{BW}(\theta_N)^3. \tag{5}$$

Equation (5) can be solved with respect to the angle θ_N at which the nucleation event occurs,

$$\theta_N = \theta_0 + \Delta \times \sqrt{\frac{1}{3}\ln(d_0^3/V_{act})}. \tag{6}$$

As the activation volume is found to be almost independent on the number of bilayers, Eq. (6) can be simplified to $\theta_N = \theta_0 + 0.6\Delta$, which holds for all N. According to the result of our micromagnetic modeling,[13] the parameter Δ is typically in the range of $(2-5)°$, resulting in a value of about 53° for θ_N. The latter is in agreement with the TEM results presented above.

The acquired data, $H_F(H_C;N)$, allows estimating the stability factor, β (Table I), which is found to be higher than 75 even for the thinnest investigated magnetic film. The value is high enough to fulfill the thermal stability requirement for recording media.[7]

V. CONCLUSIONS

We have presented a study on the influence of magnetostatic coupling on the magnetization reversal in Co/Pd

TABLE I. Coercive field (H_C), fluctuation field (H_F), activation volume (V_{act}), and thermal stability factor ($\beta=H_C/H_F$) evaluated at a reverse field equal to the coercive field for $[Co/Pd]_N$ multilayers with $N=16$, 45, and 80. The volume of an individual nanocap (V_{cap}) on the spherical particles with a diameter of 58 nm is given for comparison.

Numbers of bilayers, N	H_C (kOe)	H_F (Oe)	V_{act} (nm^3)	V_{cap} (nm^3)	β
80	4.3	55	2.1×10^3	590×10^3	78
45	5.0	60	1.9×10^3	340×10^3	83
16	5.3	48	2.4×10^3	120×10^3	110

multilayer films grown on assemblies of spherical polystyrene particles. The magnetostatic coupling was altered by changing the particles size as well as by varying the number of bilayers in the $[Co/Pd]_N$ stack. The decrease in the particle size results in an enhancement of the out-of-plane coercivity of the array of nanocaps accompanied with a substantial broadening of the switching field distribution. The latter is attributed to the increased particle size distribution for smaller particles (for the same number of bilayers) as well as to the dipolar broadening with increasing number of bilayers due to the enhanced magnetostatic interaction between neighboring nanocaps in the array. In addition, a detailed analysis of MFM images suggests a nucleation dominated reversal process located at the nanocap positions. This result is in agreement with integral magnetization measurement for estimating the activation volume responsible for the magnetization reversal. The study reveals that the activation volume is substantially smaller compared to the volume of the entire nanocap and is found to be almost independent of the number of bilayers in the stack. The latter indicates an inhomogeneous magnetization reversal process within each individual nanocap in agreement with results based on micromagnetic simulations.

ACKNOWLEDGMENTS

We would like to thank D. Suess (TU Wien) and P. Krone (TU Chemnitz) for fruitful discussions and support with micromagnetic modeling. This work was financially supported in part by the European Commission via the MAFIN Project No. 026513 and the Emmy-Noether program of the DFG.

*Corresponding author; denys.makarov@physik.tu-chemnitz.de

[1] W. U. Huynh, J. J. Dittmer, and A. P. Alivizatos, Science **295**, 2425 (2002).
[2] E. Lancelle-Beltran, P. Prene, C. Boscher, P. Belleville, P. Buvat, S. Lambert, F. Guillet, C. Boissiere, D. Grosso, and C. Sanchez, Chem. Mater. **18**, 6152 (2006).
[3] A. Baeumner, Food Technol. **58**, 51 (2004).
[4] J. Fu, B. B. Park, G. Siragusa, L. Jones, R. Tripp, Y. Zhao, and Y. J. Cho, Nanotechnology **19**, 155502 (2008).
[5] B. D. Terris and T. Thomson, J. Phys. D **38**, R199 (2005).
[6] D. Weller and T. McDaniel, in *Advanced Magnetic Nanostructures*, edited by D. Sellmyer and R. Skomski (Springer, US, 2006).
[7] S. N. Piramanayagam, J. Appl. Phys. **102**, 011301 (2007).
[8] S. N. Piramanayagam and K. Srinivasan, J. Magn. Magn. Mater. **321**, 485 (2009).
[9] R. Wood, J. Magn. Magn. Mater. **321**, 555 (2009).
[10] B. D. Terris, J. Magn. Magn. Mater. **321**, 512 (2009).
[11] P. Krone, D. Makarov, T. Schrefl, and M. Albrecht, J. Appl. Phys. **106**, 103913 (2009).
[12] M. Albrecht, G. Hu, I. L. Guhr, T. C. Ulbrich, J. Boneberg, P. Leiderer, and G. Schatz, Nature Mater. **4**, 203 (2005).
[13] T. C. Ulbrich, D. Makarov, G. Hu, I. L. Guhr, D. Suess, T. Schrefl, and M. Albrecht, Phys. Rev. Lett. **96**, 077202 (2006).
[14] M. M. Soares, E. de Biasi, L. N. Coelho, M. C. dos Santos, F. S. de Menezes, M. Knobel, L. C. Sampaio, and F. Garcia, Phys. Rev. B **77**, 224405 (2008).
[15] P. Kappenberger, F. Luo, L. J. Heyderman, H. H. Solak, C. Padeste, C. Brombacher, D. Makarov, T. V. Ashworth, L. Philippe, H. J. Hug, and M. Albrecht, Appl. Phys. Lett. **95**, 023116 (2009).
[16] T. C. Ulbrich, D. Assmann, and M. Albrecht, J. Appl. Phys. **104**, 084311 (2008).
[17] R. Micheletto, H. Fukuda, and M. Ohtsu, Langmuir **11**, 3333 (1995).
[18] D. M. S. Bagguley, W. A. Crossley, and J. Liesegang, Proc. Phys. Soc. London **90**, 1047 (1967).
[19] J. R. Childress, J. L. Duvail, S. Jasmin, A. Barthelemy, A. Fert, A. Schuhl, O. Durand, and P. Galtier, J. Appl. Phys. **75**, 6412 (1994).
[20] B. N. Engel, C. D. England, R. A. Van Leeuwen, M. H. Wiedmann, and C. M. Falco, Phys. Rev. Lett. **67**, 1910 (1991).
[21] F. J. A. den Broeder, W. Hoving, and P. J. H. Bloemen, J. Magn. Magn. Mater. **93**, 562 (1991).
[22] T. Suzuki, Scr. Metall. Mater. **33**, 1609 (1995).
[23] D. Weller, L. Folks, M. Best, E. E. Fullerton, B. D. Terris, G. J. Kusinski, K. M. Krishnan, and G. Thomas, J. Appl. Phys. **89**, 7525 (2001).
[24] J. E. Davies, O. Hellwig, E. E. Fullerton, G. Denbeaux, J. B. Kortright, and K. Liu, Phys. Rev. B **70**, 224434 (2004).
[25] O. Hellwig, A. Berger, J. B. Kortright, and E. E. Fullerton, J. Magn. Magn. Mater. **319**, 13 (2007).
[26] T. Thomson, G. Hu, and B. D. Terris, Phys. Rev. Lett. **96**, 257204 (2006).
[27] O. Hellwig, A. Berger, T. Thomson, E. Dobisz, Z. Z. Bandic, D. S. Kercher, and E. E. Fullerton, Appl. Phys. Lett. **90**, 162516 (2007).
[28] C. Bran, A. B. Butenko, N. S. Kiselev, U. Wolff, L. Schultz, O. Hellwig, U. K. Rössler, A. N. Bogdanov, and V. Neu, Phys. Rev. B **79**, 024430 (2009).
[29] Z. Málek and V. Kamberský, Czech. J. Phys. **8**, 416 (1958).
[30] O. Hellwig, A. Berger, and E. E. Fullerton, J. Magn. Magn. Mater. **290-291**, 1 (2005).
[31] D. Navas, F. LIlievski, and C. A. Ross, J. Appl. Phys. **105**, 113921 (2009).
[32] D. Makarov, E. Bermúdez-Ureña, O. G. Schmidt, F. Liscio, M. Maret, C. Brombacher, S. Schulze, M. Hietschold, and M. Albrecht, Appl. Phys. Lett. **93**, 153112 (2008).
[33] L. Néel, J. Phys. Radium **11**, 49 (1950).
[34] E. P. Wohlfarth, J. Phys. F: Met. Phys. **14**, L155 (1984).
[35] R. Street and J. C. Woolley, Proc. Phys. Soc., London, Sect. A **62**, 562 (1949).